

A time-domain method for analyzing the ship roll stabilization based on active fin control

Neha Patil^a and Suresh Rajendran^{*}

Department of Ocean Engineering, Indian Institute of Technology, Chennai – 600036, India

(Received April 17, 2021, Revised August 15, 2021, Accepted August 19, 2021)

Abstract. The present work focuses on the development of a numerical body nonlinear time-domain method for estimating the effect of active roll fin stabilizers on ship roll motion in both regular and irregular seaway. The time-domain analysis aims at providing fast and accurate ship responses that will be useful during the design process through accurate estimation of the environmental loads. A strip theory-based approach is followed where the Froude-Krylov and hydrostatic forces are calculated for the exact wetted surface area for every time step. The equations of motions are formulated in the body frame and consider the six degrees of coupled motions. The active fin, rudder, and propeller modules are included in the simulation. This leads to accurate modeling of the system dynamics. The numerical unstabilized roll motion is validated with experimental seakeeping simulations conducted on a Coastal Research Vessel (CRV). The phenomena of Parametric Rolling (PR) is identified during the numerical investigation of the candidate vessel. Besides, a nonlinear PID (NPID) control technique and LQR method is implemented for active roll motion control and its performance is observed in regular as well as irregular waves. The proposed numerical approach proves to be an effective and realistic method in evaluating the 6-DoF coupled ship motion responses.

Keywords: CRV; fin controller; irregular waves; non-linear seakeeping; NPID Controller; roll motion stabilization; parametric rolling

1. Introduction

Ships are expected to operate in different sea conditions and speed ranges. The safety and operation effectiveness of the ships are very important and they depend on effective prediction and modeling of the ship dynamics. The real-time operating environment is highly complex and nonlinear. Many researchers have developed and implemented numerous ship motion/response prediction techniques based on the level of complexity and accuracy of the sea-keeping problem.

1.1 Seakeeping time-domain numerical methods

The numerical methods can be categorized into frequency domain (FD) and time-domain (TD) methods. The TD methods can be further categorized into strip theory based methods (Fonseca and Soares 1998, Mikami and Shimada 2006, Rajendran *et al.* 2016), 3D Panel methods (Kring *et al.*

^{*}Corresponding author, Assistant Professor, E-mail: sureshr@iitm.ac.in

^a Ph.D. Student, E-mail: neha.patil0603@gmail.com

1997, Shao and Faltinsen 2014) RANSE based CFD approach (El Moctar *et al.* 2017, Oberhagemann 2016, etc. for linear and nonlinear prediction cases.

The numerical methods like the nonlinear 3D time-domain method and CFD-based methods give accurate results, however, they become highly computationally expensive and time-consuming if implemented to replicate the uncertainties of the real-environment seakeeping problem. Thus, it is very important to implement a simplified and robust method for numerical predictions which should be accurate enough for practical engineering applications. This paper highlights the development of a body nonlinear time-domain approach, based on strip theory, applied to estimate the roll motion in various heading, speed, and sea conditions.

1.2 Roll stabilization techniques

Among the three degrees of freedom with restoring coefficients, roll motion is critical because of the low damping value. The prediction and control of roll motion are of prime importance as it affects the vessel performance in terms of passenger safety, onboard operations, and vessel safety. The ship motion response predictions and the stabilization of the excessive rolling motion have been studied in the past. The area of research is still popular due to the challenges and complexities associated with the effective predictions and applications of motion control systems. To reduce the roll motion, roll stabilizers have been used for decades in the industry. The roll stabilizers are mainly classified into two groups – active and passive roll stabilizers. The passive devices operate without any power source and control system like bilge keels, passive anti-roll tanks, fixed fins, etc. The active devices produce a moment to oppose the roll motion through active control surfaces like active fins, active anti-rolling tanks, and gyroscope.

Cox and Lloyd (1977) gave a detailed paper about the hydrodynamic design and performance analysis of the different types of stabilizing devices like bilge keels, anti-roll tanks, and fins. They addressed the need for roll stabilization in the early ship design process. The development of ship motion prediction methods is important to apply advanced stabilizing devices. Zhu and Katory (1998) presented a linear time-domain analytical method to predict forces and motions using 3-D time domain Green's function. Dallinga (1993) explored the hydro-mechanical aspects of the design of fin stabilizers in terms of fin area, hull-fin interfaces, and performance of fins. Sgobbo and Parsons (1999) presented a Multiple Input Multiple Output (MIMO) controller for ship roll stabilization with fin/rudder. The modeling of ship dynamics in single and multiple degrees of freedom, wave disturbance model, and control algorithm was described in detail. Gaillarde (2002) studied the effects of mechanical angle saturation and stall condition for fins working at a lower angle of attacks and operating at low speed in mild sea conditions. The lift and drag forces were presented for three different vessels to explain the dynamic behavior of the fins. Perez and Goodwin (2008) presented a model predictive control (MPC) technique to a decoupled roll motion model to take into account the effect of dynamic stall of the fin stabilizers when the ship is operating in severe sea states. The paper discusses the non-linear effects and unsteady hydrodynamics observed in ship and fin response.

The conventional controllers or the control techniques are not effectively applied in the complex environment. Hence, the conventional controllers are replaced with advanced modern controllers in recent years. The modern controllers work based on the modern control theories – Linear Quadratic Regulator (LQR) Controller, Sliding Mode Controller, Model Predictive Controller, Integrated Controller, etc. Carletti *et al.* (2010) presented the design of an integrated control system for heading and roll damping control using fins and rudder. The ship dynamics are modeled for sway, roll, and yaw coupled motion with a nonlinear multivariable approach. Lee *et al.* (2011) designed and

numerically simulated a frequency weighted LQR controller using a combination of fin stabilizers and pod propellers for ship roll stabilization. They further compared the designed controller with a simple LQR controller. Kim and Kim (2011) presented a design for fin stabilizers using PID and LQR control techniques for decoupled roll motion and roll and pitch coupled motion. The numerical investigation was carried out with help of a sea-keeping program based on 3D Rankine panel method with time-domain formulation. Perez and Blanke (2012) discussed the control aspects and feasibility of the roll motion control devices. They discussed the limitations, constraints, and performance assessment of the control techniques for linear 1DoF and 4DoF motion models. Lavieri *et al.* (2012) applied the sliding mode technique to develop a controller for roll stabilization which was chosen to deal with the uncertainties present in the mathematical model due to inaccurate estimation of the hydrodynamic parameters and changes in the real environment. They presented computational simulations to test the designed controller for regular wave conditions. The study could be further extended to improve the efficiency of the controller and the effect under irregular waves. Ronghui *et al.* (2015) presented the control design for an uncertain nonlinear ship roll stabilization system. The neural network approach is used to approximate the unknown nonlinear parameters of the system. The proposed design is numerically validated for a sinusoidal wave disturbance for a container ship operating at design speed. Christina Kazantzidou *et al.* (2018) presented a control technique that integrates the fin and rudder for roll motion stabilization and course keeping. The ship dynamics are described with a restricted 3DoF linear model and the internal model control technique is used to design the controller. The design is investigated with simulation results for sinusoidal and stochastic disturbances in quartering, beam, and bow seas. Zhang *et al.* (2019) investigated the effect of rudders on ship roll reduction control during ship turns. The nonlinear 4-DOF motion model for a multipurpose naval vessel with forces and moments caused by hydrodynamics, propellers, rudders, and waves is established. Based on the simulation analysis of ship turning motion with static and dynamic rudder angles, a linear quadratic regulator (LQR) controller is developed to realize the rudder roll stabilization (RRS) control during turning. The extended literature review identifies the research gap in this area.

1.3 Parametric rolling

Finally, we look into the realm of parametric rolling with the developed tool. Since the numerical method takes account of the body nonlinearity, it can identify the vulnerability of the ship to parametric rolling (PR). PR occurs due to large variation in the metacentric height (GM) when a ship travels in the head or following seas. This is largely reported for containerships because container ships are slender in shape and characterized by the large bow flare which results in a significant change in the waterplane area as the wave travels along with the ship (Turk 2012), (Greco *et al.* 2015), (Somayajula and Falzarano 2014), (Rajendran and Guedes Soares, 2017). However, such a phenomenon is not limited to containerships. The candidate research vessel used in this paper has a low block coefficient and is also vulnerable to parametric rolling. International Maritime Organization (IMO) proposes 3 levels of scrutiny to check the vulnerability to parametric rolling. If a vessel is found susceptible in the first two preliminary level investigations, the vessel needs to be examined using the level 3 method, which is the direct assessment of the parametric rolling using any numerical tool. The numerical tool developed here will be suitable for such a task.

1.4 The main contributions of the paper

The previous researchers on fin-stabilization have focused on linear and nonlinear control techniques, however, the wave loads were mostly considered to be linear. This results in uncertainty in the system dynamics modeling and additional effort is required from the controller to nullify the uncertainty in nonlinear wave force modeling. In this paper, we integrate a body nonlinear time domain with control algorithms for analyzing the fin roll stabilization performance of a ship. In this way, the hydrodynamic modeling is accurate enough for engineering applications. Integration with such a numerical tool, the controller can be tuned and its effectiveness can be checked for realistic sea conditions a priori to seagoing and the optimum controller action can be decided. Additionally, as the present study deals with nonlinear motions, the linear control techniques would prove effective only over a limited operating range when applied to nonlinear systems. Hence, it is important to consider the nonlinearities in the feedback while applying a control technique. The present work focuses on the design and application of active fin stabilizers with nonlinear PID control techniques to stabilize the roll motion. The proposed control strategy works effectively in controlling the effects of parametric rolling also.

The paper is divided into the following sections: 2) The theory behind the body nonlinear time-domain (TD) formulation and the modeling of the control surfaces 3) Control system modeling which includes LQR and nonlinear PID 4) Description about the ship and wave particulars 5) In this section results and discussion are held which include 5a) the TD code results in very low wave steepness is compared with FD results and validated 5b) the TD code results are compared with experimental results for higher wave steepness 5c) Identification of parametric rolling and its control 5d) responses in irregular waves and roll stabilization based on different control algorithms.

2. Time-Domain (TD) approach

Two kinds of frames of reference are followed in this paper 1) an inertial frame – XYZ-fixed on earth and 2) the body frame - xyz. The formulation in the body frame helps to reproduce the exact body kinematics and easy integration of the control surface forces/moments. The inertial frame and the body frame coincide with each other at the starting of the simulation. The frame is located at the mean water level and the midship. A right-handed coordinate system is followed in which the positive X and Y axis point toward the bow and port direction. Positive Z-axis is upward. The same follows for the body frame. The transformation between the inertial frame and the body frame is

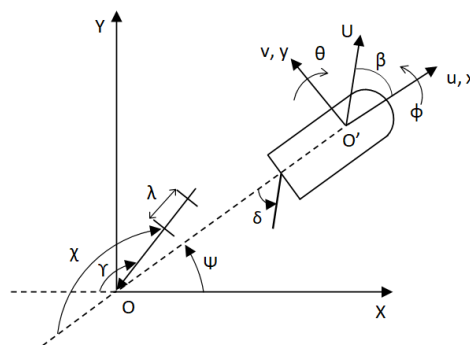


Fig. 1 Frame of Reference

carried out through Euler angles, R . Formulation in the body frame help to reproduce the exact body kinematics and easier integration of control surface forces and moments.

The 6-DoF equation of motion is given by –

$$\dot{\eta} = R(\eta)v \tag{1}$$

$$[M]\dot{v} + [C_{RB}]v = \{F_P\} + \{F_R\} + \{F_{Fin}\} + \{F_{Rest}\} + \{F_{FK} + F_D + F_{Rad}\}_i \tag{2}$$

where $i = 1,2, \dots 6$

The mass matrix is given as

$$M = \begin{bmatrix} M & 0 & 0 & 0 & M_{Z_c} & 0 \\ 0 & M & 0 & -M_{Z_c} & 0 & M_{x_c} \\ 0 & 0 & M & 0 & -M_{x_c} & 0 \\ 0 & -M_{Z_c} & 0 & I_4 & 0 & -I_{46} \\ M_{Z_c} & 0 & -M_{x_c} & 0 & I_5 & 0 \\ 0 & M_{x_c} & 0 & -I_{46} & 0 & I_6 \end{bmatrix} \tag{3}$$

The Coriolis component matrix is given by-

$$C_{RB} = \begin{bmatrix} 0 & -M_r & M_q & 0 & 0 & 0 \\ M_r & 0 & -M_p & 0 & 0 & 0 \\ -M_q & M_p & 0 & 0 & 0 & 0 \\ 0 & 0 & 0 & 0 & -I_{46}q + I_6r & -I_5q \\ 0 & 0 & 0 & -I_6r + I_{46}p & 0 & I_{46}r + I_4p \\ 0 & 0 & 0 & I_5q & I_{46}r - I_4p & 0 \end{bmatrix} \tag{4}$$

$$R(\eta) = \begin{bmatrix} c\psi & -s\psi c\theta + c\psi s\theta s\phi & s\psi s\phi + c\psi c\phi s\theta \\ s\psi c\theta & c\psi c\phi + s\phi s\theta s\psi & -c\psi s\phi + s\theta s\psi c\phi \\ -s\theta & c\theta s\phi & c\theta c\phi \end{bmatrix} \tag{5}$$

where $\ddot{\eta}_k, \dot{\eta}_k, \eta_k$ denote the acceleration, velocity, and displacement, respectively in the inertial frame, of the k mode of motion of the ship. M is the mass matrix. Roll viscous damping is included in the numerical simulation. The viscous damping factor is included in the $[B]$ matrix. The external forces and moments denoted by $\{F_P\}, \{F_R\}, \{F_{Fin}\}, \{F_{Rest}\}, \{F_{FK}\}, \{F_D\}$ and $\{F_{Rad}\}$ show the propeller thrust, rudder forces/moments, roll fin forces/moment, restoring force/moments, Froude-Krylov forces/moment, diffraction forces/moments and radiation forces/moments respectively. The added mass and damping coefficients are calculated based on the 2D panel method (Bertram *et al.* 2006), and the forward speed correction is applied based on STF theory (Salvansen *et al.* 1970). The diffraction and radiation forces are assumed to be linear.

The Froude-Krylov exciting force/moment and the restoring forces are calculated for the exact wetted surface area and hence assumed to be body nonlinear. The ship is discretized along the length into a finite number of strips. The Section curves defining the cross-section of each strip are further discretized into a finite number of line segments. The surface elevation of the wave is calculated as

$$\eta = A\cos(-kX\cos\gamma + kY\sin\gamma + \omega t + \epsilon) \tag{6}$$

where A is the wave amplitude, ω is the frequency of the incident wave, k is the wavenumber and ϵ is the phase difference. The sectional Froude-Krylov forces/moments in the inertial frame are given by

$$f_r^I(\vec{X}, t) = \rho g A e^{kz} \cos(-ikX \cos\gamma + kY \sin\gamma + \omega t + \epsilon) N_r dl \quad (7)$$

where X, Y, Z are the instantaneous position of the midpoint of the line segments in a strip (section) in the inertial frame ($\vec{X} = X\vec{i} + Y\vec{j} + Z\vec{k}$). N_r is the outward normal of the line segments in the inertial frame. The sectional forces in body frame are given as

$$f_r^B(x, t) = \sum_{i=1}^n R^{-1} f_r^I, r = 1, 2, 3 \quad (8)$$

where n is the number of line segments in a strip. The Froude-Krylov sectional moments in the body frame is given by

$$f_k^B(x, t) = \sum_{i=1}^n \vec{r} \times f_r^B, k = 4, 5, 6 \quad (9)$$

where \vec{r} is the position vector of the line segments in each strip. The Froude-Krylov forces/moments are integrated for each time instant

$$F_j^B(t) = \int_L f_j^B(x, t) dx, j = 1 \text{ to } 6 \quad (10)$$

The heave restoring forces (in the inertial frame) acting on the line segment of a strip is

$$r_3^I(\vec{X}, t) = \rho g Z N_z dl \quad (11)$$

The heave, roll and pitch restoring forces/moments in the body frame are given by Eqs. (12)-(14)

$$R_3^B(t) = \int_{x_{a2}}^{x_{f2}} [\sum_{port}^{stdb} [r_3^B]] dx - W_3 \quad (12)$$

$$R_4^B(t) = - \int_{x_{a2}}^{x_{f2}} [\sum_{port}^{stdb} [zr_2^B - yr_3^B]] dx - W_2 z_c \quad (13)$$

$$R_5^B(t) = - \int_{x_{a2}}^{x_{f2}} [\sum_{port}^{stdb} [xr_3^B]] dx - W_3 x_c + W_1 z_c \quad (14)$$

The weight vector W is given as ($\vec{W} = \vec{W}_1 i + \vec{W}_2 j + \vec{W}_3 k$). The diffraction forces are calculated based on STF theory (Salvansen *et al.* 1970), therefore assumed to be linear. The total diffraction forces/moments are calculated by integrating the sectional forces/moments over the ship length as given below

$$h_j(x) = \omega_0 e^{-ikx \cos\gamma} \int_{C_x} (in_3 - n_2 \sin\gamma) e^{iky \sin\gamma} e^{kz} \psi_j dl \quad (15)$$

$$D_j(t) = \text{Re} [\rho A e^{i(\omega_e t + \epsilon)} \int_L h_j dx], j = 2, 3, 4 \quad (16)$$

$$D_5(t) = \text{Re} \left[\rho A e^{i(\omega_e t + \epsilon)} \int_L \left[x h_3 + \frac{U}{i\omega_e} h_3 \right] dx \right] \quad (17)$$

$$D_6(t) = \text{Re} \left[\rho A e^{i(\omega_e t + \epsilon)} \int_L \left[x h_2 + \frac{U}{i\omega_e} h_2 \right] dx \right] \quad (18)$$

where ψ_j is two dimensional velocity potential, n_2 and n_3 are the unit outward normal vectors in y and z directions respectively, ω_e is the encounter frequency and x is the moment arm.

The radiation forces/moments are assumed to be linear and are calculated based on Cummins formulation (Cummins 1964).

$$F_j^{Rad}(t) = A_{jk}^\infty \dot{v}_k(t) + \int_0^t K_{jk}(t - \tau) v_k(\tau) d\tau \quad j, k = 1 \text{ to } 6 \quad (19)$$

where A_{jk}^∞ is the infinite frequency added mass and $K_{jk}(t - \tau)$ is the memory function calculated from the frequency-dependent damping coefficients. (Rajendran *et al.* 2015).

2.1 Rudder, propeller and roll stabilizing fins

The rudder module considers the hull-rudder interaction and the resulting forces and moments are calculated (Skejjic and Faltinsen 2008). Rudder modeling helps to include the additional roll moment due to the rudder. The rudder is controlled with a PD Controller with gain values - $K_{PR} = 5.35$ and $K_{DR} = 2.5$ where K_{PR} and K_{DR} are proportional and derivative gains for rudder respectively.

The rudder forces and moments are given as

$$X_R = -(1 - t_R) F_N \sin \delta \quad (20)$$

$$Y_R = -(1 + a_H) F_N \cos \delta \quad (21)$$

$$N_R = -(x_R + a_H \times x_H) (lbp) F_N \cos \delta \quad (22)$$

$$K_R = -(1 + a_H) (y_R) (lbp) F_N \cos \delta \quad (23)$$

where, F_N is rudder normal force, t_R is steering resistance deduction factor, a_H is rudder increase factor, x_H is the non-dimensional longitudinal coordinate of the acting point of the additional lateral force, x_R and y_R are the longitudinal and lateral coordinates of the rudder respectively and δ is the rudder angle.

The rudder normal force is given as

$$F_N = 0.5 \rho A_R \left(\frac{6.13 \Lambda}{\Lambda + 2.25} \right) [(u_R)^2 + (v_R)^2] \sin \alpha_R \quad (24)$$

where, A_R is profile area of the rudder, Λ is the rudder aspect ratio, α_R is effective inflow angle to the rudders ($\alpha_R = \delta - \delta_R$), δ_R is effective rudder angle at which the rudder normal force becomes zero, γ_R and l_R are flow straightening factors due to lateral speed and yaw rate respectively ($l_R \cong 2x_R$), u_p is longitudinal inflow velocity to the propeller, ε is the ratio of wake fractions, κ is a constant, and η is the ratio of the diameter of the propeller to rudder span. The rudder particulars and interaction parameters are calculated for the rudder.

A pair of B-series propellers are designed for the candidate vessel. The open water characteristics of the propeller are evaluated by performing an open water test. Hydrodynamic force due to propellers

$$F_p = (1 - t_p) \rho n_p^2 D_p K_T \quad (25)$$

where, D_p is the diameter of the propeller, n_p is the number of revolutions (rps), t_p is thrust deduction factor and K_T is thrust coefficient. The rudder and propeller data is given in the tables below

The important parameters in the fin design are the fin size (profile area) and the fin location. A series of geometrically symmetric airfoil sections, NACA four-digit series for low Reynolds number

application is used in the present design. The fin is located at the midship. The location of the fin close to the center of gravity ensures the minimum coupling with the other motions (Dallinga 1993) (Gaillard 2002). The fin parameters are as mentioned in Table 6. The lift and fin moment is given by

$$Lift = \frac{1}{2} \rho V^2 S C_L \quad (26)$$

The restoring moment produced by the fin is given by

$$E_{fin} = 2 * Lift * L_y * \cos \left[\text{atan}^{-1} \left(\frac{V_y}{V_x} \right) \right] \quad (27)$$

where α is the fin angle of attack, C_L is the coefficient of lift and S is the fin planform area. The incoming flow speed, V is given as

$$V = (V_x, V_y) = (U - u_w(t), \dot{z} + \dot{\phi} L_y - \dot{\theta} L_x - v_w(t)) \quad (28)$$

Table 1 Rudder Particulars

Particulars	Value
Span	0.092 m
A_R	0.0168 m ²
Aspect ratio	1.167
x_R	-0.472
y_R	0.249

Table 2 Parameters for calculating rudder forces

Particulars	Value
α_H	0.0858
t_R	0.4404
x_H'	-0.4371
ε	0.9
κ	0.59
γ_R	0.5317
l_R'	-0.9436

Table 3 Propeller data

Particulars	Value
Diameter	0.12m
Pitch ratio (P/D)	0.90
Expanded blade area ratio (A_e/A_o)	0.60
Hub diameter ratio	0.20
x_p	-0.462
y_p	0.244

Table 4 Predicted Parameters for propeller forces

Particulars	Value
J_0	0.3984
J_1	-0.2997
J_2	-0.1405
n_p	1.65
t_p	0.21
w_{p0}	0.0726

Table 5 Fin Particulars

Particulars	For prototype (43m)
Number of fins	2
Planform area	4 m ²
Aspect ratio	1
Profile	NACA 0015

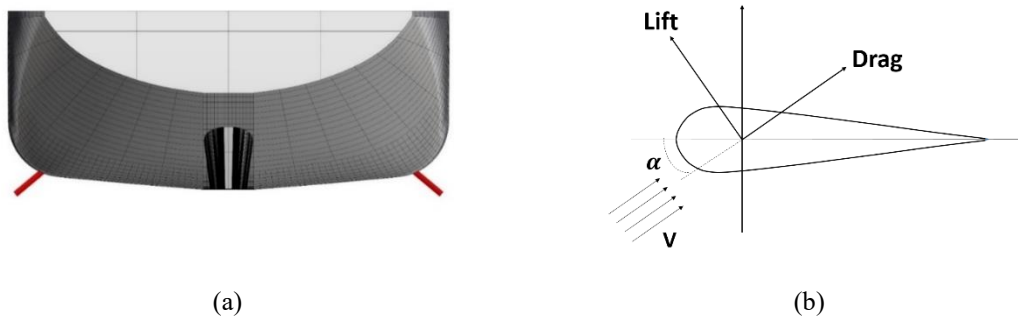


Fig. 2 Typical arrangement of the fins (a) and schematic of fin forces (b)

where U is the ship forward speed, u_w and v_w are horizontal and vertical components of the fluid particle velocities respectively, L_x and L_y are fin moment arms. ϕ and θ are the roll and pitch angles. The fin effective angle is given by

$$\alpha = \text{fin angle} + \theta + \left[\text{atan}^{-1} \left(\frac{v_y}{v_x} \right) \right] \tag{29}$$

3. Control system

The vessel experiences a high magnitude of roll motion in beam sea condition which needs to be controlled. The vessel is analyzed for a linear control application and further compared with the nonlinear feedback control application. A linear quadratic regulator (LQR) control technique is implemented for its robustness and optimality over traditional linear controllers.

3.1 Linear quadratic regulator

The roll motion model is locally linearized at the resonance frequency and coupled for 3DoF sway, roll, and yaw motion for control application. The Eq. (2) is rearranged as

$$\dot{v} = [M + A(\omega)]^{-1}(F_{ext} - C_{RB}v - Bv) \quad (30)$$

where the mass matrix is given as

$$M = \begin{bmatrix} M & -M_{Z_c} & M_{x_c} \\ -M_{Z_c} & I_4 & -I_{46} \\ M_{x_c} & -I_{46} & I_6 \end{bmatrix} \quad (31)$$

The Coriolis component matrix is given by

$$C_{RB} = \begin{bmatrix} 0 & 0 & 0 \\ 0 & -I_{46}q + I_6r & 0 \\ 0 & 0 & 0 \end{bmatrix} \quad (32)$$

F_{ext} represents the combined external excitation forces. The above equation is modeled in state-space form as given below

$$\dot{x} = Ax + Bu \quad (33)$$

$$y = Cx \quad (34)$$

The state matrix is given as $x = [y \ y \ \phi \ \dot{\phi} \ \psi \ \dot{\psi}]^T$, A is the state matrix, B is the input matrix, C is the output matrix and the controller input is $u = -Kx$. The feedback gain matrix K is calculated by solving the linear quadratic cost function. The cost function is given as

$$J = \int_0^{\infty} (x^T Qx + u^T Ru) dt \quad (35)$$

where Q is the state-cost weighted matrix and R is the control weighted matrix. The LQR controller aims at minimizing the cost function to give an optimal controller output by tuning Q and R weighting matrices. The R matrix alters the control signals – a larger R -value means the system is stabilized with less energy, that is, an expensive control strategy and a lower R -value means the control signal is not penalized, that is, cheap control strategy. The R matrix also depends on the actuator saturation limits. The Q matrix alters the states of the system – a larger Q value corresponds to a lesser change in the states of the system. As a trade-off between the two, the Q matrix is fixed as an identity matrix or a function of $C'C$ matrix, and the R matrix is altered to obtain the desired control response. The matrix R is chosen to be $R = [1.5]$ and the matrix $Q = pC'C$ where p is the weighting factor which is modified to obtain the desired step response as given in Fig. 3 while tuning the controller.

3.2 Nonlinear feedback control

The linear control techniques may be suitable for moderate operating conditions and may behave poorly when the system is subjected to uncertainties and non-linearity. The control system can be improved for its cost and efficiency by implementing a nonlinear PID control technique, in which, the gain is calculated based on the system response. The present NPID technique considers the

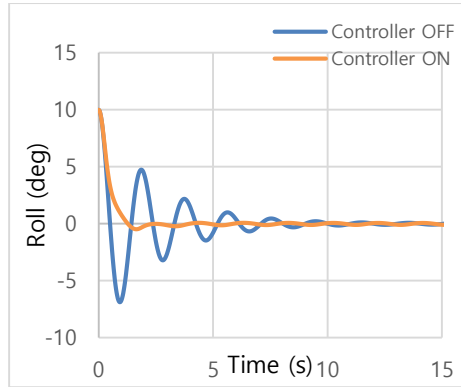


Fig. 3 Roll decay response for the vessel with and without control action

feedback function as a continuous dynamic function (Tian *et al.* 1999). The controller gain value, integral time, and derivative time are calculated as nonlinear functions of the error signal e .

The NPID controller is represented as

$$u(t) = K_P(e) \left[e(t) + \frac{1}{T_I(e)} \int_0^t e(t) dt + T_D(e) \frac{de(t)}{dt} \right] \quad (36)$$

where $u(t)$ is the controller input, $K_P(e)$ is the controller gain, $T_I(e)$ and $T_D(e)$ are the nonlinear integral time and derivative time respectively. The controller gain is presented as the function of error signal e ,

$$K_P(e) = K_{Pmax} - (K_{Pmax} - K_{Pmin})(1 + a_p|e|)\exp(-a_p|e|) \quad (37)$$

where K_{Pmax} and K_{Pmin} are the maximum and minimum values of the controller gain such that $K_{Pmax} \geq K_P \geq K_{Pmin}$ and a_p is a positive parameter. Similarly, the $T_I(e)$ and $T_D(e)$ values are calculated as

$$T_I(e) = T_{Imax} - (T_{Imax} - T_{Imin})(1 + a_i|e|)\exp(-a_i|e|) \quad (38)$$

$$T_D(e) = T_{Dmax} - (T_{Dmax} - T_{Dmin})(1 + a_d|e|)\exp(-a_d|e|) \quad (39)$$

where T_{Imax} , T_{Dmax} and T_{Imin} , T_{Dmin} are the maximum and minimum values of the integral time and derivative time respectively such that, $T_{Imax} \geq T_I \geq T_{Imin}$ and $T_{Dmax} \geq T_D \geq T_{Dmin}$. a_D and a_I are positive parameters. The base values for the controller gain and time are tuned based on the open-loop and closed-loop step response observations of the linearized system (1DoF in roll motion) as given by the transfer function

$$G_{\phi w} = \frac{k_\phi w_n^2}{s^2 + 2\xi w_n s + w_n^2}$$

The transfer function is analyzed for the roll resonance condition frequency of $w_n = 3.21$ rad/s. The closed-loop response for the linear transfer function is initially plotted for a proportional gain value of 1. The proportional gain value is tuned to obtain the system oscillations for a given constant amplitude. The derivative and integral gains are tuned to adjust the desired response time and settling error of the system. The linear PID gain values help to decide the maximum and minimum values for the controller gain of the NPID controller. The linear PID gain values are also

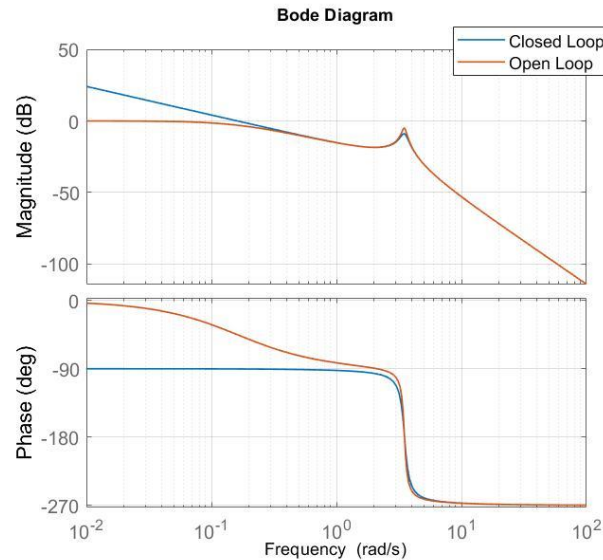


Fig. 4 Bode Diagram

verified with a linear 6DoF system. The gain set for the NPID controller is then finalized based on the gains for 1DoF and 6DoF model-based PID controllers.

The roll decay plot (Fig. 3) and the bode plot (Fig. 4) depict the effectiveness, stability, and margins of the open-loop and closed-loop system. Fig. 3 shows the comparison of roll damping response for the vessel with and without the control action. The vessel is subjected to an initial inclination of 10deg and then allowed to attain the equilibrium position (0deg). The plot depicts the effectiveness of NPID control action on the roll damping performance of the vessel. Fig. 4 shows the phase margin and gain margin of the open-loop and closed-loop system. The gain margin of the system is ~ 16 dB and the phase margin is 89.7° . The system is in a stable loop. It can be observed that the peak magnitude decreases for the controller action in closed-loop which shows the damping effect imposed by the fin-based control system.

The Eqs. (37)-(39) depict that the controller gains are evaluated based on the control error signal. If the value of the error signal is higher, the values of $K_P(e)$, $T_I(e)$ & $T_D(e)$ are also higher and vice versa. Therefore, the control input signal is automatically estimated based on the error value.

4. Experimental setup

A free-running model of a Coastal Research Vessel (CRV) is used for seakeeping tests (Dubey and Subramanian 2017). The seakeeping tests are performed in a 30 m length x 30 m width x 3 m water depth Wave Basin facility of the Department of Ocean Engineering, IIT Madras. A scaled-down model of CRV (1:17) is used for the model tests. The model is tested for beam sea conditions in regular waves with a wave steepness of $1/50$ ($\frac{\text{wave height}}{\text{wave length}} = 1/50$). The roll natural period of the vessel is 7.83s. The vessel particulars and the incident regular wave details are given below.

Table 6 Vessel Particulars

Particulars	Prototype (43 m)		Model (1:17)	
Length overall, LOA	43	m	2.529	m
Beam	9.6	m	0.565	m
Draft	2.5	m	0.147	m
Depth	3.70	m	0.217	m
Displacement	615950	Kg	121.95	kg
Froude number	0.1		0.1	
Metacentric height (GM)	0.739	m	0.0435	m
LCG from aft perpendicular	17.696	m	1.041	m

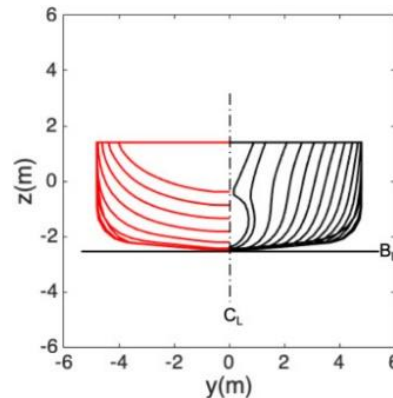


Fig. 5 The fabricated model and the body plan of the vessel (Subramanian *et al.* 2020)

5. Results

The simulations are carried out to investigate ship roll response in regular waves. It is important to observe the ship roll response close to its natural period and investigate the ship behavior in a resonance condition when the motions are severe. The simulation results are presented for different wave headings, frequencies, wave steepness, and ship speeds in the form of Response Amplitude Operators (RAOs). All the data given below are on the Prototype scale.

The RAOs are calculated as given below

$$Roll\ RAO = \frac{Roll\ Amplitude\ (rad)}{Wave\ Slope} \tag{40}$$

where, $Wave\ Slope = k \eta_a$, k and η_a are the wave number and wave amplitude.

The numerical simulation is conducted for $F_n = 0$ and the speed corresponding $F_n = 0.1$ for three headings. Beam Sea (90°) and Oblique Sea (135°) and Head Sea (180°) are considered to investigate the effectiveness of the nonlinear time-domain approach over a wide range of applications. The heave, roll, and pitch motion responses are investigated for these cases. The results include simulations for the ship responses in low and high wave steepness and roll motion control applications. The low steepness waves ($H/L = 1/200$) are compared with the linear frequency-

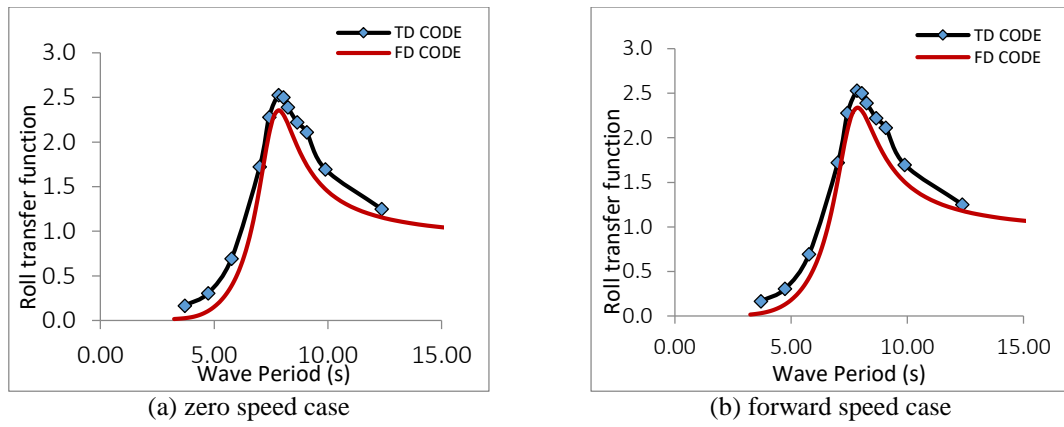


Fig. 6 Roll RAOs for 90° heading for zero speed (a) and forward speed (b) condition

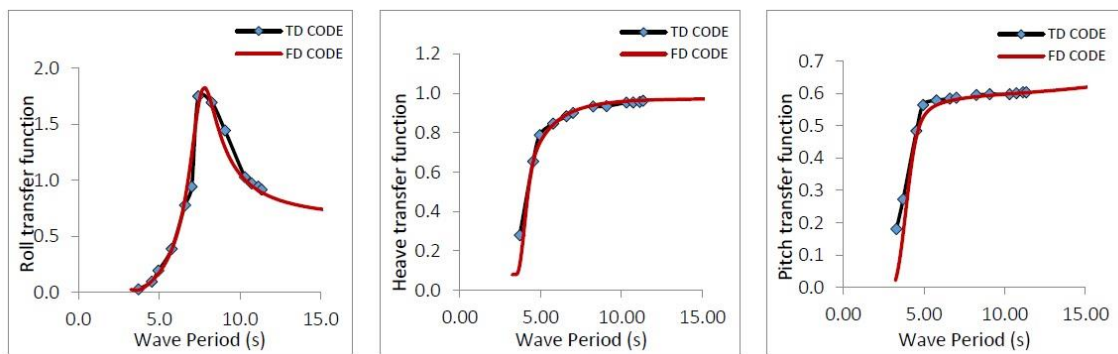


Fig. 7(b) Roll, Heave and Pitch RAOs for 135° heading zero speed condition

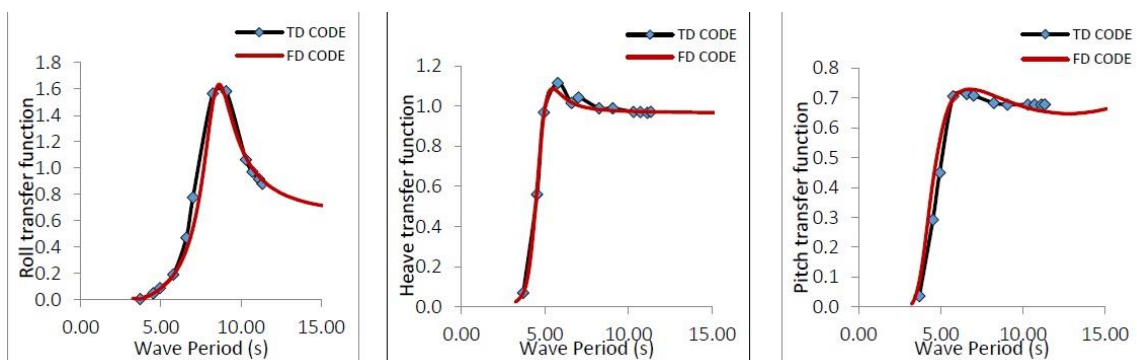


Fig. 7(b) Roll, Heave and Pitch RAOs for 135° heading forward speed condition

domain code (Figs. 6-8) and the high steepness waves ($H/L = 1/50$) are compared with the experimental simulations performed in the wave basin facility (Fig. 9).

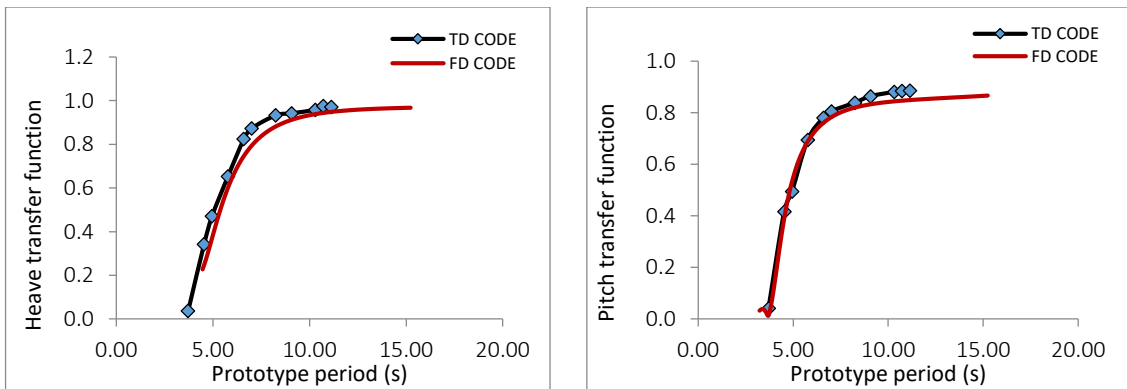


Fig. 8 (a) Heave and Pitch RAOs for 180° heading zero speed condition

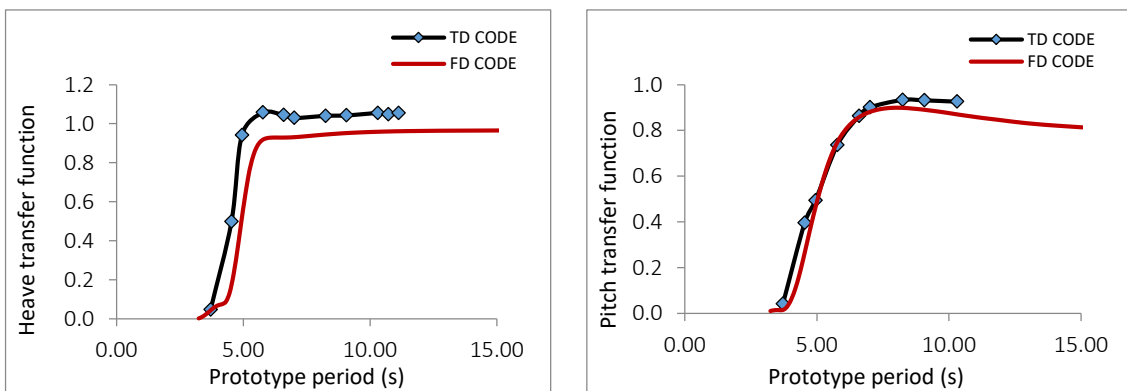


Fig. 8 (b) Heave and Pitch RAOs for 180° heading forward speed condition

5.1 Comparison with Frequency Domain (FD) results for low wave steepness ($H/L = 1/200$)

In this section, the time domain results are validated by comparison with the frequency domain (FD) results for low wave steepness ($H/L = 1/200$) for both zero speed condition and steady speed condition (forward speed case). The frequency-domain results are obtained from STF theory (Salvensen *et al.* 1970). For a very low steepness, the nonlinear TD code and FD code results should match.

Fig. 6 shows the comparison between TD and FD results for the roll transfer function for 90° heading for zero speed case and forward speed case plotted against the wave period. Ikeda formula (Ikeda *et al.* 1978) gives a roll viscous damping factor of 0.05. However, the roll viscous damping factor based on the experiment is found to be 0.07, which is used in the numerical simulation. The roll resonance occurs at 7.83s and the heave peak occurs at 4.79s. These values match with the natural frequency calculations i.e., $\omega_n = \sqrt{\frac{K}{M}}$, where K is the heave/roll stiffness and M is the summation of mass/roll mass moment of inertia and the associated added mass/roll added inertia.

The FD roll RAO peak values are slightly lower than TD results, however, the difference between them is less than 10%. The model in the time domain simulation is subjected to sway and yaw motion

and the restoring forces are calculated for the exact wetted surface area. This may lead to a slight difference between the FD and TD results based on the exact location of the ship in the inertial frame.

Figs. 7(a) and 7(b) shows the comparison of FD and TD motion RAOs in 135° wave heading for zero speed and forward speed condition. The roll RAO peak value has decreased by 30% and 12% in the oblique sea for zero and forward speed conditions, respectively. The heave and pitch RAOs for the forward speed are characterized by resonance peaks. Figs. 8(a) and 8(b) depict heave and pitch plots for 180° heading and the TD code results are in good agreement with the FD code results. There is a slight discrepancy between FD and TD RAO for forward speed conditions in head seas. However, the difference is less than 10%.

5.2 Comparison of RAOs with Experimental results for wave steepness $H/L=1/50$

Fig. 9 depicts the Roll RAOs for zero speed case and forward speed case for wave heading - 90° . The Time Domain (TD) Code and Experiments are investigated for a wave steepness of $1/50$ (wave height/ wavelength). As the wave steepness increases, the ship is subjected to larger sway and yaw motions and also drifts, which affect the roll motion. Even though second-order drift forces are not included in the calculation, a component of the drift force results from the body nonlinear estimation of the Froude-Krylov forces. Therefore, to estimate the roll RAO, the average amplitude of the last 6 cycles of roll motion is considered. The roll RAO in beams seas slightly decreases by 6% when compared to Fig. 6 (low wave steepness). There is a good agreement between the TD and the experimental results for the roll RAO in beam seas.

The TD and experimental Roll RAO peak occur at 8.25s. The difference in the resonance frequency values between the low ($1/500$) and high ($1/50$) wave steepness cases is less than 5%. This slight difference is probably due to the nonlinear restoring force which may lead to a change in the instantaneous position of the metacentric height. The TD RAO peak value in steeper waves is 8% smaller than the low amplitude waves. This is probably due to the nonlinear effects which the TD code can capture. Similar behavior for heave and pitch responses of a containership in the extreme sea was reported by Dalzell (1962). RAO peaks increase with speed i.e. by 11 and 14%, respectively, for the numerical and experimental cases. The TD code slightly overestimates the experimental RAO peak values however it's less than 8%.

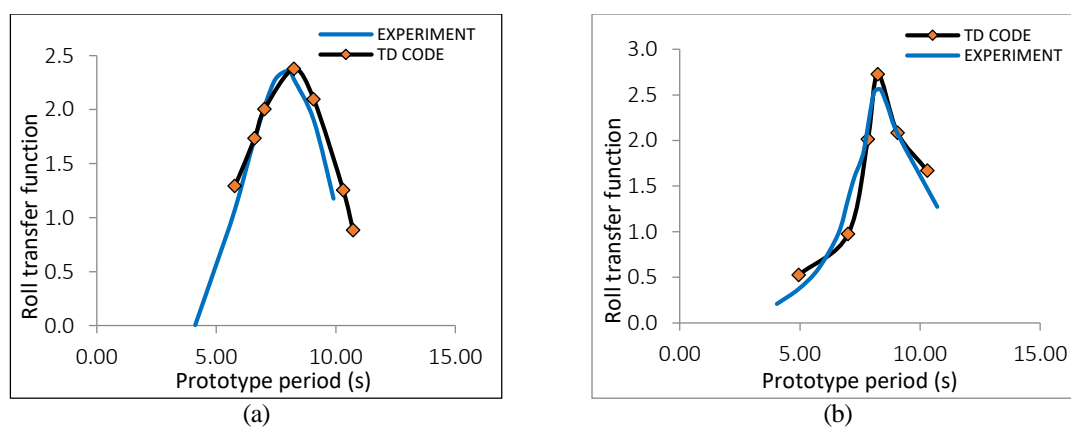


Fig. 9 Roll RAOs for 90° heading for zero speed (a) and forward speed (b) condition

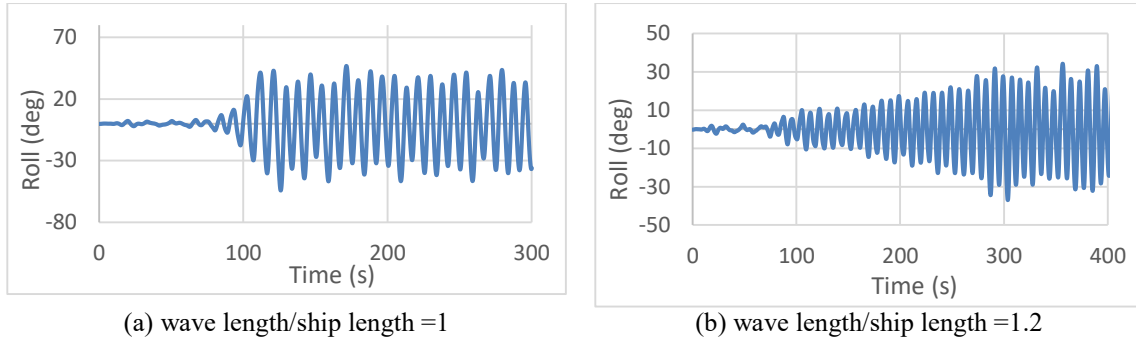


Fig. 10 Parametric Rolling identified in vessel subjected to wave steepness = 1/12 and 180° heading

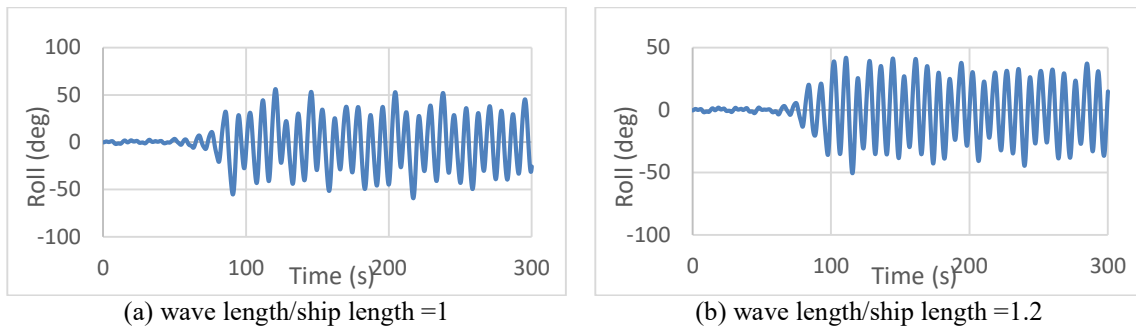


Fig. 11 Parametric Rolling identified in vessel subjected to wave steepness = 1/12 and 170° heading

5.3 Parametric rolling

During parametric rolling, a ship is subjected to heavy rolling due to parametric excitation in head seas. Generally, the problem is approached as a Mathieu-type instability in which the nonlinear dynamics are represented by a 1DoF nonlinear roll equation of motion. Even though such methods are effective in predicting the vulnerability to parametric rolling, the roll amplitude estimation may not be accurate. As the roll motion is coupled with other modes in a highly nonlinear motion, the prediction of coupled modes is necessary for accurate prediction. Since the TD code incorporates body nonlinear restoring forces, it's able to identify parametric rolling. The CRV model used here is tested higher wave steepness (1/12) and found to be vulnerable to parametric rolling in the head seas for a wave to ship length ratio of 0.8, 1 and 1.2 ($\frac{\lambda}{L_{pp}} = 0.8, 1 \text{ and } 1.2$). The parametric rolling generally occurs when the encountering frequency is double the roll natural frequency (i.e., $\omega_e \sim 1.6 \text{ rad/s}$). When the ship encounters waves with $\frac{\lambda}{L_{pp}} \sim 1$ and a Froude number of 0.1, the encountering frequency matches the criterion. Figs. 10 and 11 show the ship roll response in 180 and 170 degrees, respectively. The phase plane plot in Fig. 12 shows the boundedness of the responses.

5.4 Roll stabilization using active fin control system for 6-DoF model

5.4.1 Ship response in regular waves

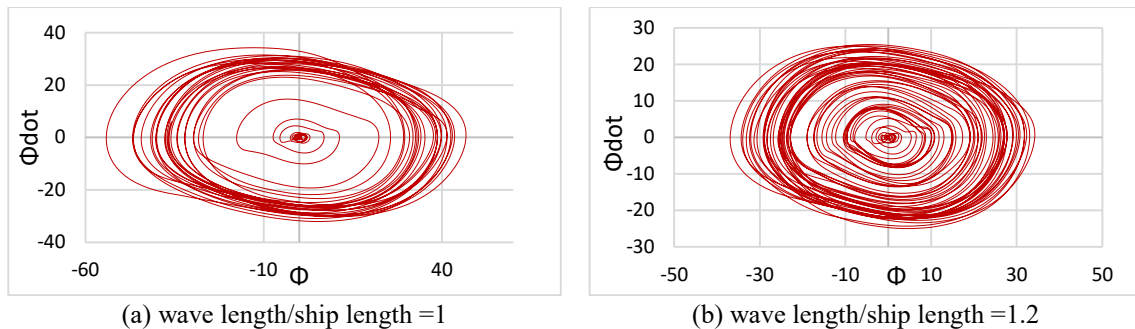


Fig. 12 Phase Plot for vessel subjected to wave steepness = 1/12 and 180° heading

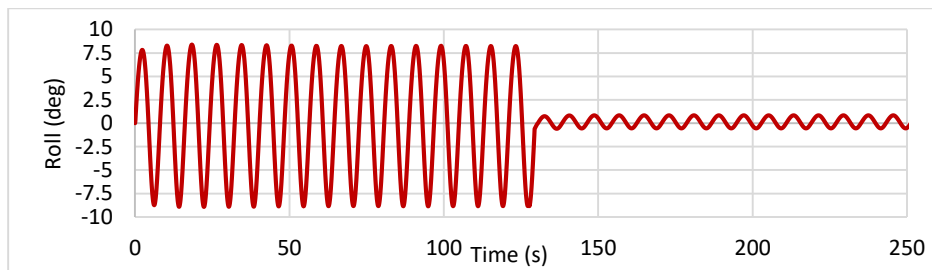


Fig. 13 Controlled and uncontrolled roll motion response at the resonance frequency

The roll motion time series for beam seas and the resonance frequency corresponding to the natural roll period are plotted in Fig. 13. The propeller rpm is set to 610 RPM to achieve a speed of 2 m/s. The time series is plotted for a regular wave with wave slope = 1/50 and the wavelength/ship length ratio is 2.6 which matches the roll resonance frequency. In this case, the ship response with maximum roll magnitude is observed. The ship roll motion is controlled with the help of a fin-based nonlinear PID (NPID) controller. The controller is tuned for the gain values of $K_{Pmax} = 15$, $K_{Pmin} = 8.5$, $T_{Imax} = 6.5$, $T_{Imin} = 4.5$, $T_{Dmax} = 12.5$ and $T_{Dmin} = 6.5$. The positive parameters a_p , a_I and a_D are set to 1. The fin angle is constrained to $\pm 20^\circ$. The controller is switched ON at 100s.

Fig. 13 shows that the maximum uncontrolled roll amplitude observed in the case of resonance condition is 7.96° . The NPID controller controls the roll amplitude to 0.84° and thus a roll reduction of 89.44% is achieved.

Figs. 14(a) and 14(b) depict the Roll RAO for 90° and 135° heading (wave slope = 1/50) for Fin ON and Fin OFF case for forward speed condition. The Fin ON case represents the roll motion stabilization with the active fin controller switched ON and the Fin OFF case represents the roll response of the vessel without the action of any roll stabilizing device. The comparison of the RAOs shows a significant reduction in the roll magnitude when the controller is active.

Figs. 15(a) and 15(b) depict the Parametric Roll time series for 180° and 170° heading (wave slope = 1/12, wavelength/ship length = 1) for Fin ON and Fin OFF case for forward speed condition. The plots depict that the excessive parametric rolling amplitude is effectively stabilized with the proposed NPID controller.

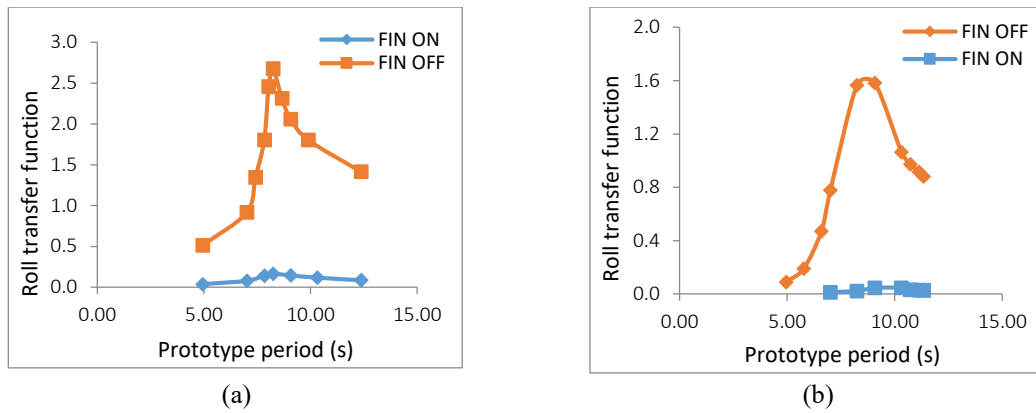


Fig. 14(a) Roll RAO for 90° heading and (b) Roll RAO for 135° heading

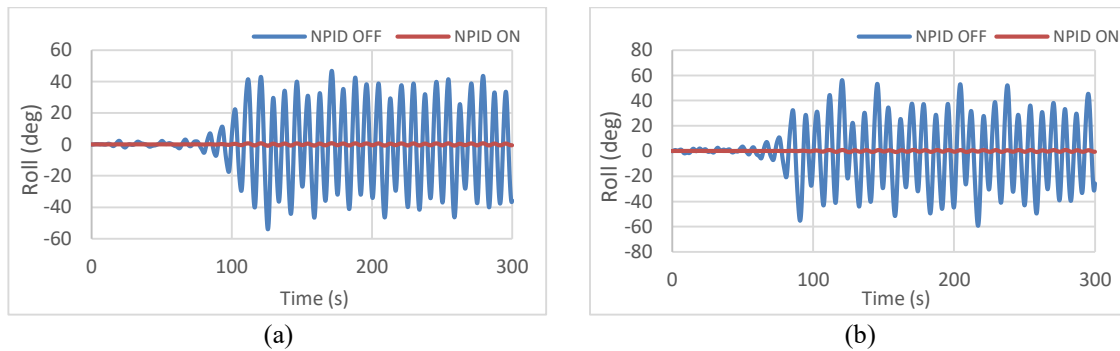


Fig. 15(a) Parametric Roll Stabilization with fin control for 180° heading and (b) Parametric Roll Stabilization with fin control for 170° heading

Table 8 Summary of parametric rolling simulation data

Heading	Wave Length / Ship Length ratio	Parametric Roll (PR) Amplitude (deg)	Stabilized Parametric Roll Amplitude (deg)	
			LQR	NPID
170°	0.8	No PR	-	-
	1	39.66	1.50	1.41
	1.2	32.84	1.46	1.32
180°	0.8	No PR	-	-
	1	43.11	1.65	1.60
	1.2	29.65	1.34	1.15

Table 9 presents the summary of results. The table includes the roll stabilization tests performed for wave slopes 1/10, 1/20, and 1/50 and wave headings of 45°, 90°, and 135°. The % Roll Reduction in both the cases is more than 89% for all the cases.

Table 9 Summary of roll response in regular waves (Prototype Scale)

Wave Slope	Wave length/Ship length ratio	Heading	ω_e^* (rad/s)	Roll Magnitude (deg)		% Roll Reduction
				Controller OFF	Controller ON	Controller ON
1/10	1	45°	1.036	Capsizes	1.98	-
	1	90°	1.259	Capsizes	1.34	-
	1	135°	1.483	Capsizes	1.12	-
1/20	1	45°	1.036	12.4	1.15	90.73%
	1	90°	1.259	10.16	1.075	89.42%
	1	135°	1.483	6.1	0.64	89.51%
	1.2	45°	0.961	14.02	1.41	89.94%
	1.2	90°	1.146	12.06	1.25	89.64%
	1.2	135°	1.331	6.82	0.68	90.03%
1/50	1	45°	1.036	4.08	0.41	89.95%
	1	90°	1.259	3.71	0.35	90.57%
	1	135°	1.483	3.41	0.34	90.03%
	1.2	45°	0.961	6.44	0.62	90.37%
	1.2	90°	1.146	3.97	0.28	92.95%
	1.2	135°	1.331	2.86	0.26	90.91%
	2.6**	90°	0.777	19.28	1.78	90.77%
	3.16**	135°	0.777	18.54	1.63	91.20%

* ω_e = wave encountering frequency

**resonance condition

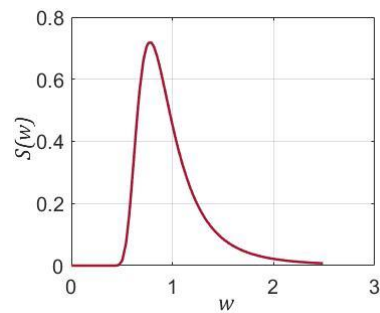


Fig. 16 Jonswap Spectrum

5.4.2 Ship responses in irregular waves

The heave, roll, and pitch motion responses are investigated for the vessel in irregular seas generated based on the Jonswap wave spectrum (Fig. 16). Figs. 17 and 18 present roll and stabilized roll, time series, and respective energy plots for vessel subjected to an irregular wave of Sea State 4 ($H_s = 2.5$ m, $T_p = 8.88$ s) and 135° wave heading and for a Froude number of 0.1. The incident wave peak frequency results in resonance condition for the aforementioned condition. All the wave input data is on a prototype scale. The peak frequency of the roll response spectrum matches with the

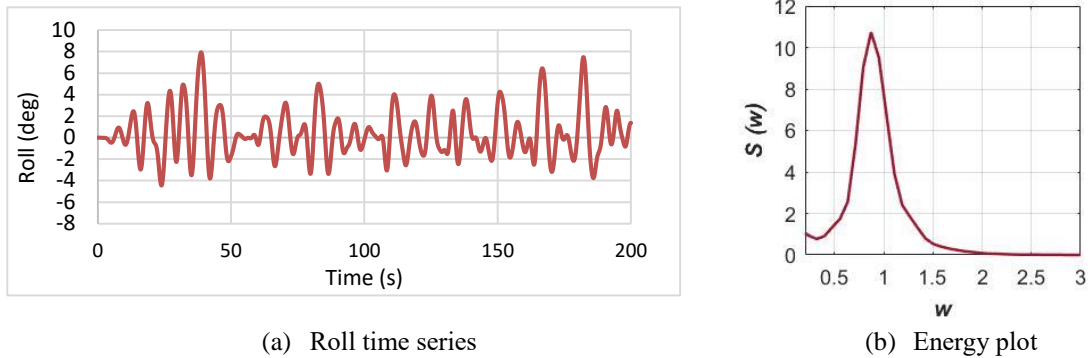


Fig. 17 Roll motion time series and energy plot for vessel subjected to Sea State 4 for 135° wave heading

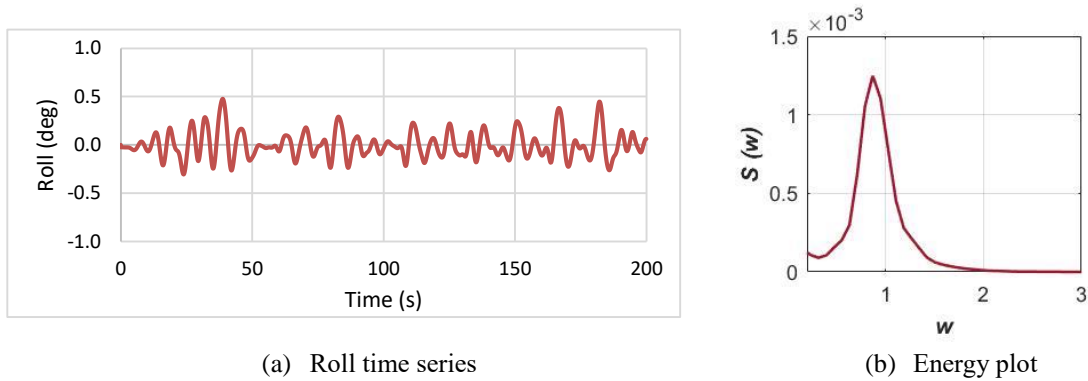


Fig. 18 Stabilized roll motion time series and energy plot for vessel subjected to Sea State 4 for 135° wave heading

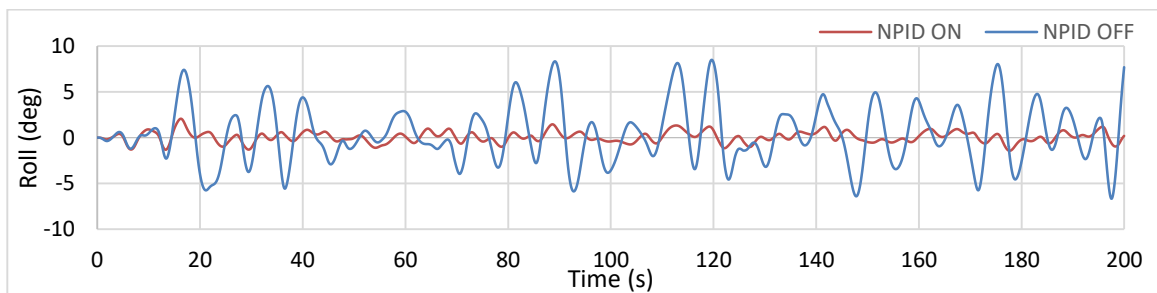


Fig. 19 Controlled and uncontrolled roll motion response for ship subjected to irregular waves at Sea State 4 and 90° wave heading.

resonance frequency. The roll energy is reduced by 97 % by the active fin stabilizer based on NPID controller.

Fig. 19 represents the comparison of roll motion time series for the vessel in an irregular seaway for controlled and uncontrolled motion. The vessel is exposed to extreme rolling conditions to investigate the effectiveness and maximum performance of the roll stabilization system.

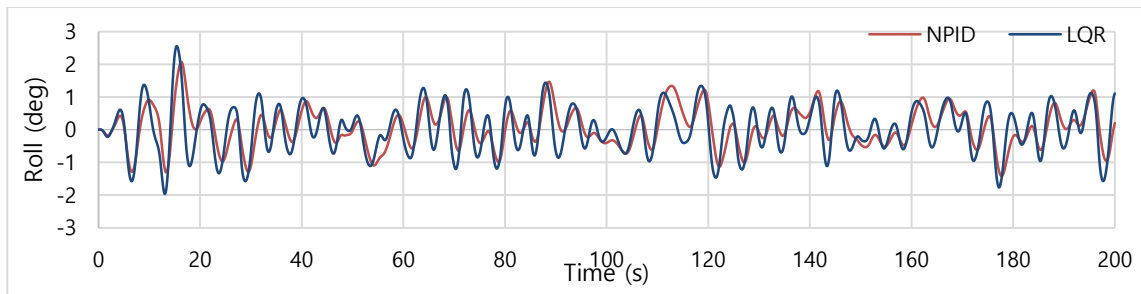


Fig. 20 Roll motion response comparison for NPID and LQR controller for the vessel in Sea State 4 and 90° wave heading

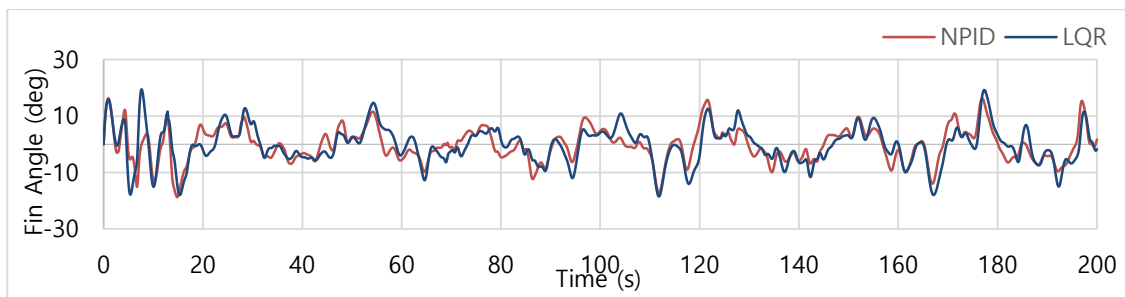


Fig. 21 Fin angle comparison for NPID and LQR controller for the vessel in Sea State 4 and 90° wave heading

Table 10 Summary of roll response in irregular waves

Heading	Wave Length / Ship Length ratio	Parameter	Mean	Variance	Skewness	Kurtosis
90	2.6*	Heave	0.0265	0.7008	0.0509	2.7703
		Roll	-0.2475	9.2396	0.3538	3.8948
		Stabilized Roll	-0.0371	0.2079	0.3538	3.8948
		Pitch	-0.0398	0.3374	0.1380	2.6908
135	3.16*	Heave	0.0177	0.4731	0.0341	2.7943
		Roll	-0.0562	1.1767	0.0583	3.2505
		Stabilized Roll	-0.009	0.0301	0.0583	3.2505
		Pitch	-0.0812	4.4419	0.0508	2.8962

*corresponds to the resonance frequency

Fig. 20 depicts the comparison of the NPID controller with a linear quadratic regulator controller. The magnitude of roll reduction for the NPID controller is slightly higher (~2% higher) than that for the linear controller for the given fin actuator constraints. There is no significant difference in the maximum roll amplitude between these two controllers.

Even though there is no significant difference in the maximum roll amplitude between NPID and LQR controller, it will be interesting to look at the fin performance based on these controllers. Fig. 21 depicts the comparison of fin angle for NPID and linear quadratic controller. The Roll RMS value before stabilization is 8.718 and that after stabilization is 0.349 with NPID controller and 0.512 with

LQR controller. The RMS value of fin deflection for NPID controller is 5.973 and that for LQR controller is 6.613 (i.e., 10% reduction for NPID). The maximum fin angle in the case of the LQR controller is 18.85° and that in the case of NPID controller is 15.67° . The maximum fin angle reduction achieved is 16.87%. The average fin angle deflection in the case of the LQR controller is 5.41° and that in the case of NPID controller is 4.61° . Therefore, the average fin angle reduction is 14.5%. Therefore, the NPID controller offers a smaller value of actuator signal i.e. fin angle without affecting the motion stabilization effectiveness. This directly contributes to the lesser energy consumption.

Table 10 summarizes the heave, roll, and pitch motion responses in irregular waves. The data is obtained for Sea State 4 ($H_s = 2.5$ m) and for an incident wave peak frequency that matches the resonance condition. The data is plotted for 1800s duration.

6. Conclusions

A roll stabilizing active fin model based on NPID control technique is coupled with a body nonlinear time domain to investigate the ship responses in a wide range of incident waves. The investigation discusses the implementation of a fin-based active controller to stabilize the roll motion responses. The numerical simulations plotted for different cases depict the versatility of the proposed techniques for different cases.

In the first part of the results section, the time domain approach is validated by comparing the results with a frequency domain approach for the low steepness wave, that is, wave height/wavelength ratio $H/L = 1/200$. Both the numerical estimations are in good agreement and consistent for all the headings for ship roll motion. Later, the time domain results are plotted for higher wave steepness ($H/L = 1/50$) to validate with the experimental results. These time-domain simulations are validated with the experimental simulations and found to be in good agreement. The TD roll RAO peak values in steeper waves decrease by 6 and 8% for beam and oblique sea conditions. In comparison with and without speed in steeper waves, the |TD RAO peaks increases by 11% following a similar trend as the experimental RAO. In the head sea condition, the time domain approach identifies the vulnerability of the ship to Parametric Rolling. The vessel is tested for a range of wave to ship length ratios that result in an encountering frequency approximately equal to double the roll natural frequency. The PR is identified in both 170 and 180 deg heading and the roll response characteristics are investigated.

The roll motion stabilization problem is addressed for the vessel operating in regular and irregular waves. The NPID controller reduces the roll by 89.44% for the resonance condition in regular waves for beam sea condition. The stabilized and unstabilized roll RAOs are compared and the effectiveness of the NPID controller is analyzed. Similarly, the NPID controller is used for stabilizing the PR and can reduce the roll motion by 89%. The proposed non-linear controller is also compared with the LQR controller. The results depict the effectiveness of the NPID over the LQR control technique.

Finally, the NPID and LQR controllers are tested for analyzing the roll response in irregular waves. The incident wave peak frequency results in resonance conditions for the tested cases. The roll energy is reduced by 97 % by the active fin stabilizer based on NPID controller. Even though there is no significant difference between the NPID and LQR performance on the roll angle reduction, the NPID controller results in reduced fin deflection for achieving the same performance. This directly contributes to the lesser energy consumption of the fin actuator mechanism.

The proposed technique of ship motion response prediction and ship motion control is effective and versatile over a wide operating range. It can be used as a computing resource for practical application to investigate the influence of the external environmental forces. The method helps to build a data bank for the controller gain which will be useful for ship navigation based on the accurate estimation of the roll motion.

Acknowledgments

We are extremely thankful to Prof. Anantha Subramanian for the experimental setup and data.

References

- Bertram, V., Veelo, B., Soding, H. and Graf, K/ (2006), "Development of a freely available strip method for seakeeping", *In COMPIT*, **6**, 356-368.
- Bhattacharyya, R. (1978), "Dynamic of marine vehicles", John Wiley & Sons, New York.
- Carletti, C., Gasparri, A., Ippoliti, G., Longhi, S., Orlando, G. and Raspa, P. (2010), "Roll damping and heading control of a marine vessel by fins-rudder VSC", *IFAC Proceedings*, **43**(20), 34-39.
- Cox G.G. and Lloyd, A.R. (1977), "Hydrodynamic design basis for navy ship roll motion stabilization", Presented at the Annual Meeting, New York.
- Dallinga, R.P. (1993), "Hydromechanic Aspects of the Design of Fin Stabilisers", RINA Spring Meetings.
- Dalzell, J.F. (1962), "Application of cross bispectral analysis to ship resistance in waves", Stevens Institute of Technology, Hoboken, New Jersey, May.
- Dubey, A.C. and Subramanian, V.A. (2017), "Wi-Fi enabled autonomous ship model tests for ship motion dynamics and seakeeping assessment", *IIRE J. Maritime Res. Develop.*, 1(2).
- El Moctar, O., Ley, J., Oberhagemann, J. and Schellin, T.E. (2017), "Nonlinear computational methods for hydrodynamic effects of ships in extreme seas", *Ocean Eng.*, **130**, 659-673.
- Fonseca, N. and Guedes Soares, C. (1998), "Time-domain analysis of large-amplitude vertical ship motions and wave loads", *J. Ship Res.*, **42**(2), 139-152.
- Fossen, T.I. (1994), "Guidance and Control of Ocean Vehicles", John Wiley & Sons.
- Gaillarde G. (2002), "Dynamic behaviour and operational limits of stabiliser fins", IMAM, Creta.
- Greco, M., Lugni, C. and Faltinsen, O.M. (2015), "Influence of motion coupling and nonlinear effects on parametric roll for a floating production storage and offloading platform", *Philos. T. R. Soc. A*, 373, 20140110.
- Ikeda, Y., Himeno, Y. and Tanaka, N. (1978), "A prediction method for ship roll damping", Technical Report, University of Osaka Prefecture, Osaka.
- Kazantzidou, C., Perez, T., Donaire, A. and Valentinis, F. (2018), "Internal model control for rudder roll stabilization and course keeping of a surface marine craft", *IFAC-Papers on Line*, **51**(29), 457-462.
- Kim, Y., Kim, K., Kim, J., Kim, T., Seo, M. and Kim, Y. (2011), "Time-domain analysis of nonlinear motion responses and structural loads on ships and offshore structures: development of WISH programs", *Int. J. Naval Archit. Ocean Eng.*, **3**(1), 37-52.
- Kring, D., Huang, Y., Scalavounos, P., Vada, T. and Braathen, A. (1997), "Nonlinear ship motions and wave induced loads by a Rankine method", *Proceedings of the 21st symposium naval hydrodynamics*.
- Lavieri, R.S., Getschko, N. and Tannuri, E.A. (2012), "Roll stabilization control system by sliding mode", *IFAC Proceedings*, **45**(27), 447-452.
- Lee, S., Rhee, K.P. and Choi, J.W. (2011), "Design of the roll stabilization controller, using fin stabilizers and pod propellers", *Appl. Ocean Res.*, **33**(4), 229-239.
- Li, R., Li, T., Bai, W. and Du, X. (2016), "An adaptive neural network approach for ship roll stabilization via

- fin control”, *Neurocomput.*, **173**, 953-957.
- Lloyd, A.R.J.M. (1975), “Roll stabilizer fins: A design procedure”, R. Instit. Nav. Architects, suppl. Papers; G.B., **117**, 233-254.
- Mikami, T. and Shimada, K. (2006), “Time-domain strip method with memory-effect function considering the body non-linearity of ships in large waves”, *J. Mar. Sci. Technol.*, **11**(3).
- Oberhagemann, J. (2016), On Prediction of Wave-Induced Loads and Vibration of Ship Structures with Finite Volume Fluid Dynamic Methods, University of Duisburg-Essen, Duisburg. Doctoral Thesis.
- Perez, T. and Blanke, M. (2011), “Ship roll damping control”, *Annu. Rev. Control*, **36**(1), 129-147.
- Perez, T. and Goodwin, G.C. (2008), “Constrained predictive control of ship fin stabilizers to prevent dynamic stall”, *Control Eng. Practice*, **16**(4), 482-494.
- Rajendran, S. and Guedes Soares, C. (2017), “Numerical investigation of parametric rolling of a container ship in regular and irregular waves”, *Proceedings of the ASME 2017 36th International Conference on Ocean, Offshore and Arctic Engineering. American Society of Mechanical Engineers Digital Collection*.
- Rajendran, S., Fonseca, N. and Guedes Soares, C. (2016), “Body nonlinear time domain calculation of vertical ship responses in extreme seas accounting for 2nd order Froude-Krylov pressure”, *Appl. Ocean Res.*, **54**, 39-52.
- Salvensen, N., Tuck, E.O. and Faltinsen, O. (1970), “Ship motions and sea loads”.
- Sgobbo, J.N. and Parsons, M.G. (1999), “Rudder/fin roll stabilization of the USCG WMEC 901 class vessel”, *Marine Technology and SNAME news* 36.3.
- Skejjic, R. and Faltinsen, O.M. (2008), “A unified seakeeping and maneuvering analysis of ships in regular waves”, *J. Mar. Sci. Technol.*, **13**(4), 371-394.
- Somayajula, A.S. and Falzarano, J.M., (2015), “Validation of volterra series approach for modelling parametric rolling of ships”, *Proceedings of the 34th International Conference on Offshore Mechanics and Arctic Engineering*, OMAE 2015-41528.
- Subramanian, R., Jyothish, P.V. and Subramanian, V.A. (2020), “Genetic algorithm based design optimization of a passive anti-roll tank in a sea going vessel”, *Ocean Eng.*, **203**, 107216.
- Tian, Y., Tade, M.O. and Tang, J. (1999), “A nonlinear PID controller with applications”, *IFAC Proceedings*, **32**(2), 2657-2661.
- Turk, A. (2012), “Coupled nonlinear parametric resonance model for container ships”, Doctoral dissertation. University of Rijeka, Croatia
- Zhang, S., Zhao, P. and Liang, L. (2018), “LQR-based ship roll reduction control using fin stabilizer”, *Proceedings of the 2018 IEEE International Conference on Mechatronics and Automation (ICMA)*, IEEE.
- Zhu, D.X. and Katory, M. (1998), “A time-domain prediction method of ship motions”, *Ocean Eng.*, **25**(9), 781-791.